Cellular/Molecular

Bax Interacting Factor-1 Promotes Survival and Mitochondrial Elongation in Neurons

David B. Wang,[1] Takuma Uo,[1] Chizuru Kinoshita,[1] Bryce L. Sopher,[2] Rona J. Lee,[1] Sean P. Murphy,[1] Yoshito Kinoshita,[1] Gwenn A. Garden,[2] Hong-Gang Wang,[3] and Richard S. Morrison[1]

[1]Departments of Neurological Surgery and [2]Neurology, University of Washington School of Medicine, Seattle, Washington 98195-6470, and [3]Department of Pharmacology, The Pennsylvania State University College of Medicine, Hershey, Pennsylvania 17033

Bax-interacting factor 1 (Bif-1, also known as endophilin B1) is a multifunctional protein involved in the regulation of apoptosis, mitochondrial morphology, and autophagy. Previous studies in non-neuronal cells have shown that Bif-1 is proapoptotic and promotes mitochondrial fragmentation. However, the role of Bif-1 in postmitotic neurons has not been investigated. In contrast to non-neuronal cells, we now report that in neurons Bif-1 promotes viability and mitochondrial elongation. In mouse primary cortical neurons, Bif-1 knockdown exacerbated apoptosis induced by the DNA-damaging agent camptothecin. Neurons from Bif-1-deficient mice contained fragmented mitochondria and Bif-1 knockdown in wild-type neurons also resulted in fragmented mitochondria which were more depolarized, suggesting mitochondrial dysfunction. During ischemic stroke, Bif-1 expression was downregulated in the penumbra of wild-type mice. Consistent with Bif-1 being required for neuronal viability, Bif-1-deficient mice developed larger infarcts and an exaggerated astrogliosis response following ischemic stroke. Together, these data suggest that, in contrast to non-neuronal cells, Bif-1 is essential for the maintenance of mitochondrial morphology and function in neurons, and that loss of Bif-1 renders neurons more susceptible to apoptotic stress. These unique actions may relate to the presence of longer, neuron-specific Bif-1 isoforms, because only these forms of Bif-1 were able to rescue deficiencies caused by Bif-1 suppression. This finding not only demonstrates an unexpected role for Bif-1 in the nervous system but this work also establishes Bif-1 as a potential therapeutic target for the treatment of neurological diseases, especially degenerative disorders characterized by alterations in mitochondrial dynamics.

Key words: **apoptosis; Bax interacting factor 1; Bif-1; endophilin B1; ischemia; mitochondrial dynamics**

Introduction

Bax-interacting factor-1 (Bif-1, also known as endophilin B1) was originally identified as a proapoptotic protein that binds to and activates Bax in response to apoptotic stress (Cuddeback et al., 2001). Overexpression of Bif-1 promotes apoptosis (Cuddeback et al., 2001), whereas knockdown of Bif-1 suppresses cytochrome *c* release and apoptosis (Takahashi et al., 2005). Consistent with the ability of endophilins to induce membrane curvature, Bif-1 has also been implicated in the regulation of mitochondrial morphology, as knockdown or expression of a dominant-negative form of Bif-1 resulted in elongated mitochondria in HeLa cells (Karbowski et al., 2004b).

Accumulating evidence suggests that a multitude of diseases are associated with dysfunctional regulation of mitochondrial dynamics (Schon and Przedborski, 2011). Changes in mitochondrial size and shape are regulated by the processes of fission and fusion, through the action of highly conserved dynamin-related GTPases, including dynamin-related protein 1 (Drp1) for fission and mitofusins (Mfn1 and Mfn2) for fusion (Karbowski and Youle, 2003). The size, shape, and distribution of mitochondria in neurons are especially important for neuronal survival and synaptogenesis (Schon and Przedborski, 2011; Bertholet et al., 2013). For instance, knock-out of Drp1 in mice results in abnormally large mitochondria that cannot be transported out of the soma into the processes, leading to Purkinje cell degeneration (Kageyama et al., 2012). Mitochondria in fibroblasts of these mice were normal, however, suggesting that neurons are uniquely vulnerable to changes in mitochondrial dynamics (Kageyama et al., 2012). Supporting these observations, loss-of-function mutations in dynamin-related GTPases often result in neurodegenerative phenotypes (Delettre et al., 2000; Züchner et al., 2004; Waterham et al., 2007). The levels of expression and cellular distribution of these GTPases are also affected in Alzheimer's disease and Huntington's disease (Wang et al., 2009; Kim et al., 2010), providing further support that alterations in mitochondrial dynamics may be causally related to neurodegeneration.

Received Sept. 23, 2013; revised Dec. 16, 2013; accepted Jan. 11, 2014.

Author contributions: D.B.W., Y.K., and R.S.M. designed research; D.B.W., C.K., B.L.S., R.J.L., S.P.M., Y.K., G.A.G., and R.S.M. performed research; T.U., B.L.S., and H.-G.W. contributed unpublished reagents/analytic tools; D.B.W., B.L.S., S.P.M., Y.K., G.A.G., and R.S.M. analyzed data; D.B.W., Y.K., and R.S.M. wrote the paper.

This work was supported by National Institutes of Health Grants NS35533 and NS056031 to R.S.M., by the American Heart Association Grant-in-Aid to S.P.M., and by an NINDS Institutional Center Core Grant to support the viral core facility in the Neuroproteomics Center at the University of Washington (NS055088). We thank Min Spencer for her assistance with electron microscopy.

The authors declare no competing financial interests.

Correspondence should be addressed to Dr Richard S. Morrison, Department of Neurological Surgery, University of Washington School of Medicine, Box 356470, Seattle, WA 98195-6470. E-mail: yael@u.washington.edu.

DOI:10.1523/JNEUROSCI.4074-13.2014

 0270-6474/14/342674-10$15.00/0

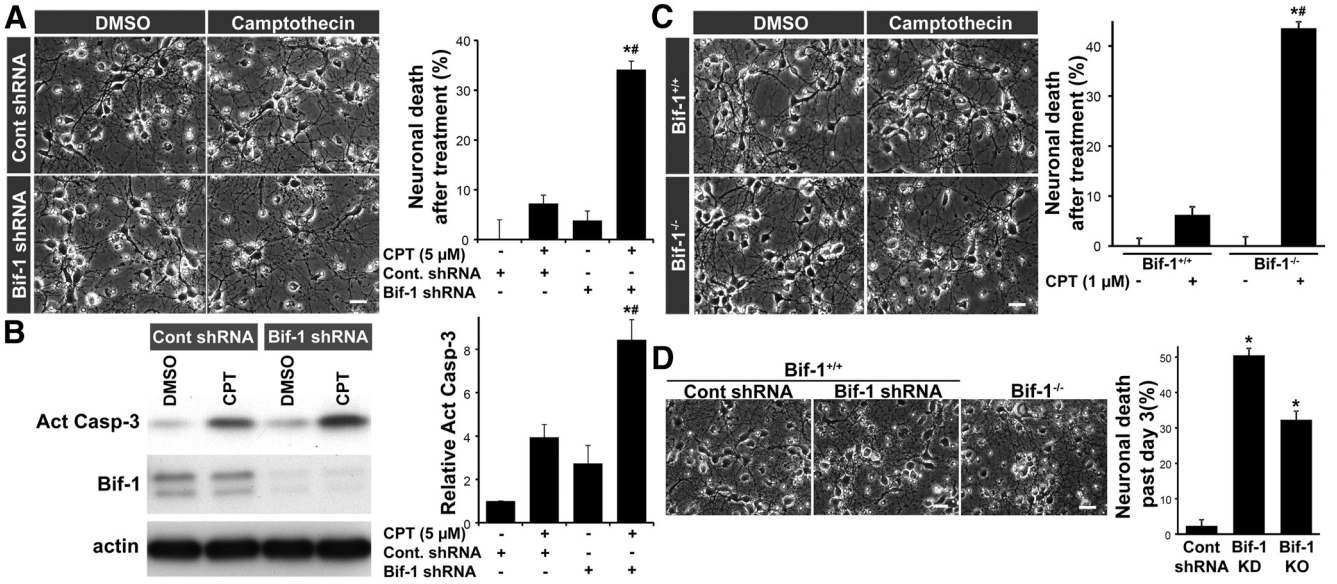

Figure 1. Bif-1 is prosurvival in neurons. ***A***, Loss of Bif-1 enhanced neuronal death caused by CPT (5 μM, 12 h). Overall neuronal viability was monitored morphologically, based on phase-contrast microscopy and nuclear morphology, as previously described (Xiang et al., 1998). Bars represent mean ± SEM ($N = 3$); *$p < 0.05$ versus CPT/control shRNA; #$p < 0.05$ versus DMSO/Bif-1 shRNA, two-way ANOVA with Tukey *post hoc* test. ***B***, Western blot analysis of activated caspase-3 expression confirmed that Bif-1 shRNA-infected neurons display increased sensitivity to CPT-induced apoptosis. Data are expressed as fold-elevation of activated caspase-3/actin relative to control (DMSO)/control shRNA. Bars represent mean ± SEM ($N = 3$); *$p < 0.05$ versus CPT/control shRNA; #$p < 0.05$ versus DMSO/Bif-1 shRNA, two-way ANOVA with Tukey *post hoc* test. ***C***, At a lower dose of CPT (1 μM, 12 h), neurons derived from Bif-1 $^{-/-}$ mice are more sensitive to CPT-induced cell death than neurons from WT Bif-1 $^{+/+}$ mice. Bars represent mean ± SEM ($N = 3$); *$p < 0.05$ versus CPT/Bif-1 $^{+/+}$; #$p < 0.05$ versus DMSO/Bif-1 $^{-/-}$, two-way ANOVA with Tukey *post hoc* test. ***D***, Knocking down Bif-1 in wild-type neurons or culturing Bif-1 $^{-/-}$ neurons for 5 d results in significant neuronal death relative to control shRNA infection of wild-type neurons. KD, Knockdown (wild-type neurons infected with Bif-1 shRNA); KO, knock-out (neurons derived from Bif-1 $^{-/-}$ mice). Bars represent mean ± SEM ($N = 3$); *$p < 0.05$ versus control shRNA infected Bif-1 $^{+/+}$ neurons, one-way ANOVA with Tukey *post hoc* test. Scale bars: ***A***, ***C***, ***D***, 25 μm. All images and blots are representative of three separate experiments.

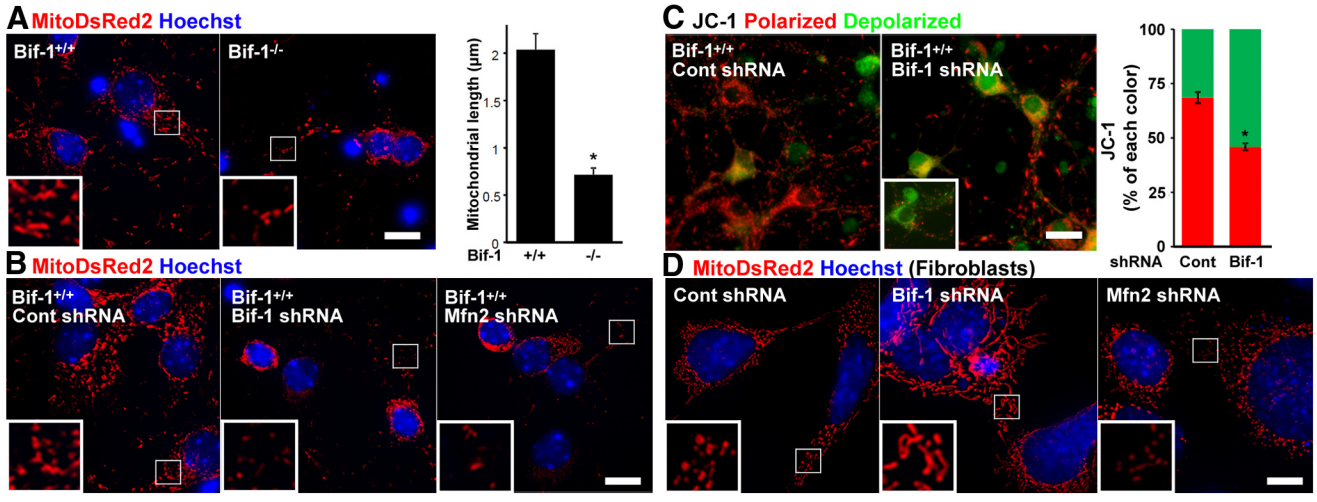

Figure 2. Loss of Bif-1 in neurons results in fragmented, depolarized mitochondria. ***A***, Mitochondria in primary postnatal cortical neurons from Bif-1 $^{-/-}$ mice, as visualized with MitoDsRed2 fluorescence, are noticeably smaller and more punctate compared with those in Bif-1 $^{+/+}$ neurons. Unlike Bif-1 $^{+/+}$ neurons, they contained more mitochondria in the perinuclear region than in neurites. Nuclei are visualized with Hoechst 33258 dye (blue). The length of individual mitochondria were outlined manually and measured using ImageJ by an observer blinded to the treatment conditions; *$p < 0.05$, Student's *t* test ($n = 3$ separate cultures). ***B***, Similar to Bif-1 $^{-/-}$ neurons, wild-type neurons infected with Bif-1 shRNA contained fragmented, punctate mitochondria that were absent from neurites. Neurons infected with Mfn2 shRNA as a positive control for induced mitochondrial fission contained similarly fragmented mitochondria indicative of mitochondrial fission, as previously reported (Uo et al., 2009). ***C***, Bif-1 knockdown resulted in mitochondrial membrane depolarization, as revealed by a red-to-green shift of JC-1 fluorescence. EGFP fluorescence, used as an infection marker of the shRNA, was very weak relative to JC-1 green fluorescence and was therefore judged as negligible. A positive control for dissipating mitochondrial membrane potential, treatment with the mitochondrial uncoupler FCCP, is shown in the inset. The data are represented as the percentage of red fluorescence intensity compared with total fluorescence intensity (red + green). Bars represent mean ± SEM; *$p < 0.05$ versus control shRNA, one-way ANOVA with Tukey *post hoc* test ($n = 3$ separate cultures). ***D***, Mouse embryonic fibroblasts infected with Bif-1 shRNA contained elongated and more interconnected mitochondria, whereas those infected with Mfn2 shRNA displayed smaller, punctate mitochondria. Scale bars: ***A***, ***B***, ***D***, 10 μm; ***C***, 20 μm. All images are representative of 2–3 separate experiments. White bordered insets demarcate areas that were magnified threefold.

In the present study, we report that Bif-1 exhibits neuron-specific functions which are opposite to what has been described for non-neuronal cells, in the regulation of apoptosis and mitochondrial morphology. Although Bif-1 knockdown in fibroblasts attenuated DNA damage-induced apoptosis and promoted mitochondrial elongation, Bif-1 knockdown in primary mouse cortical neurons increased their sensitivity to p53-dependent apoptosis and promoted mitochondrial fragmentation. Restora-

tion of Bif-1 expression in Bif-1-deficient neurons eliminated their increased sensitivity to DNA damage and corrected the mitochondrial phenotype in an isoform-specific manner. The unique Bif-1 functions observed in neurons may be explained by longer, alternatively spliced forms of Bif-1 previously identified as brain-specific (Modregger et al., 2003), which we have now demonstrated are neuron-specific. Mice lacking Bif-1 were also more sensitive to ischemic damage induced by middle cerebral artery occlusion. These findings suggest that Bif-1 promotes mitochondrial elongation and enhances cell viability in neurons, in contrast to other cell types where it acts as a mitochondrial fragmentation-promoting, proapoptotic protein. As such, the study of Bif-1 might reveal novel cell-specific modifiers of neuronal degeneration.

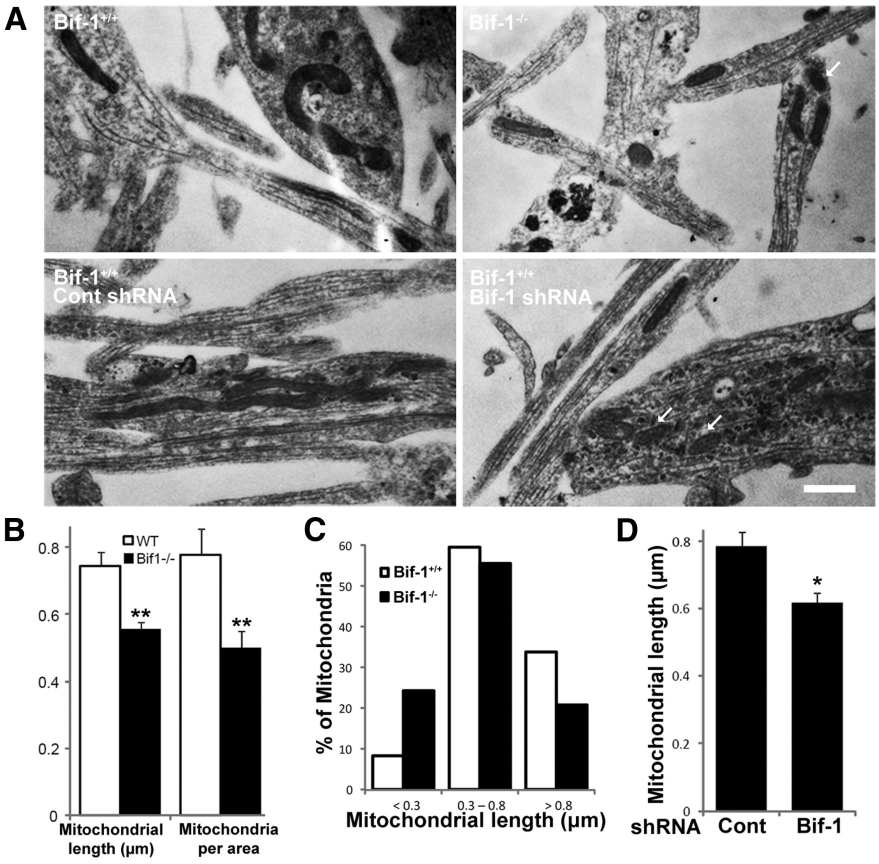

Figure 3. Loss of Bif-1 results in shorter neuritic mitochondria in cultured neurons as assessed by electron microscopy. ***A***, EM pictures show neurons cultured from Bif-1-deficient mice, and neurons from wild-type mice infected with Bif-1 shRNA, displayed smaller, fragmented mitochondria in neurites compared with relevant controls. Scale bar, 500 nm. Arrowheads represent examples of smaller, fragmented mitochondria. ***B***, Neurons cultured from Bif-1-deficient mice contain significantly smaller and fewer neuritic mitochondria compared with neurons from wild-type mice. Bars represent mean ± SEM; $^{**}p < 0.01$, Student's *t* test ($N = 20$ different images for mitochondrial length, $N = 10$ for number of mitochondria per unit neurite area, with ~150 mitochondria counted per condition). ***C***, The data in ***B*** are redrawn to show the difference in mitochondrial size distribution. Compared with wild-type controls, neurons from Bif-1-deficient mice had ~3-fold more mitochondria smaller than 0.3 μm, and 1.5-fold less mitochondria larger than 0.8 μm. ***D***, Bif-1 shRNA infection in neurons from wild-type mice also resulted in significantly smaller mitochondria compared with control shRNA infection. Bars represent mean ± SEM; $^{*}p < 0.05$, Student's *t* test ($N = 20$ images).

Materials and Methods

Animals. C57BL/6 mice were obtained from The Jackson Laboratory. Bif-1 deficient (Bif-$1^{+/-}$) mice (Takahashi et al., 2007), which had been backcrossed to C57BL/6 16 times, were obtained from Dr Hong-Gang Wang (Penn State College of Medicine). Bif-$1^{+/+}$ and Bif-$1^{-/-}$ mouse lines were derived and maintained by homozygous mating for <2 years for the present study. Genotypes were confirmed by PCR using primer sets: TGCCTCAGATGACCACCAGCCACC and TCACCACTG GGTGGAGCCGCT, or CTTAGTGAGCTGT CAGGAGAGC and AGGTTCTCATGGGA ACAGCGAC for Bif-1 wild-type and CTTAG TGAGCTGTCAGGAGAGC and TCGCC TTCTTGACGAGTTCT for Bif-1 knock-out. Mitochondrial-targeted CFP (Mito-CFP) mouse line C, which expresses mitochondrial-targeted CFP in neurons under the control of a modified Thy1 promoter (Misgeld et al., 2007), was obtained from The Jackson Laboratory and backcrossed to C57BL/6 11 times before deriving mito-CFP homozygous animals. Experiments with these animals were approved by the University of Washington institutional animal care committee.

Cell culture. Primary cultures of postnatal cortical neurons from newborn mice prenatal day (P)0 were prepared as previously described (Xiang et al., 1996). Neurons were maintained in Neurobasal-A (Invitrogen), supplemented with B-27 (Invitrogen), and GlutaMAX-I (Invitrogen). Mouse embryonic fibroblasts (MEFs) and NIH3T3 fibroblasts were prepared and/or maintained as previously described (Uo et al., 2005, 2007, 2009). When necessary, cultures were first infected with lentivirus at 10 MOI (including MitoDsRed2 for mitochondrial labeling as single or double infection) 1 d after plating (neurons) or splitting (fibroblasts). Four days after plating/splitting, cells were either harvested/fixed without treatment or treated with camptothecin (CPT; 5 μM, Sigma-Aldrich) for 12 h before harvesting/fixing, unless otherwise specified. Overall neuronal viability was monitored morphologically, based on phase–contrast microscopy and nuclear morphology, as previously described (Xiang et al., 1998). To quantitate CPT-induced death of neurons, cell viability was first determined at the time of treatment (day 3) and the baseline cell death rate (%) obtained was subtracted from the rate determined post-treatment to report the effect of CPT only on the neurons that were surviving at the time of treatment. Other cell types used for Bif-1 expression studies included primary astrocytes, spinal cord neural progenitor cells, and human SH-SY5Y neuroblastoma cells, prepared and/or maintained as previously described (Uo et al., 2005, 2007, 2009). Neuro-2a mouse neuroblastoma cells were obtained from Dr Sen-itiroh Hakomori (Pacific Northwest Diabetes Research Institute, Seattle, WA) and cultured in Eagle's minimal essential medium with 10% fetal bovine serum. Cells were harvested from exponentially growing cultures.

Plasmid construction and lentivirus production. Production of DNA constructs and lentivirus for EGFP, mitochondrial-targeted DsRed2 (MitoDsRed2), control shRNA, and Mfn2 shRNA has been previously described (Uo et al., 2009). Bif-1 shRNA plasmids were obtained from Sigma-Aldrich and one sequence (CCGGCCTACTTAGAACTTCTCAATTCTCG AGAATTGAGAAGTTCTAAGTAGGTTTTTG) validated for efficient Bif-1 knockdown was packaged into lentivirus coexpressing IRES-driven EGFP as an infection marker. Mfn2 shRNA efficacy has been previously characterized (Uo et al., 2009). The cDNA encoding human Bif-1a (NM_016009.4/NP_057093.1) was obtained from Invitrogen and cloned into pCMV-Tag2B (Stratagene) using PCR. The nucleotide sequences unique to human Bif-1b and Bif-1c (Modregger et al., 2003) were introduced into the vector using long-primer PCR. All isoforms were FLAG-tagged at the C-terminus. Plasmids were packaged into lentiviral vectors as previously described (Uo et al., 2009). All of the PCR cloned sequences in these vectors were confirmed by DNA sequence analysis.

RT-PCR for Bif-1 isoforms. RNA was isolated from brain homogenate or cell culture lysate, using an RNeasy isolation kit (Qiagen), and reverse transcribed using SuperScript II Reverse Transcriptase according to the manufacturer's instructions (Invitrogen). The cDNAs were subjected to PCR using custom murine (5′-attcaaacatcagccttaaatttcc-3′ and 5′-aagtcatctgggcttctacaaagt-3′) or human (5′-attcaaacgtcagccttaaattttc-3′ and 5′-aagtcatctgggcttctacaaagt-3′) primers designed to amplify the region encompassing exons 6 and 7. Amplification of human and mouse cDNAs with these primers yielded 304, 367, and 415 bp products from the Bif1a, Bif1b, and Bif1c isoforms, respectively. The cDNAs were subsequently cloned into pBluescript for sequencing.

Immunoblotting and immunofluorescence. Protein extracts for Western blot analysis were prepared as described previously (Uo et al., 2005). Primary antibodies used were mouse monoclonal Bif-1 (clone 30A882.1.1, 1:500; Imgenex), mouse monoclonal β-actin (clone AC-15, 1:10,000; Sigma-Aldrich), rabbit polyclonal activated caspase-3 (No. 9661, 1:1000; Cell Signaling Technology), mouse monoclonal Drp1 (clone 8/DLP1, 1:1000; BD Biosciences), rabbit monoclonal Mfn2 (clone NIAR164, 1:2000; Epitomics), mouse monoclonal Opa1 (clone 18/OPA1, 1: 5000; BD Biosciences), rabbit polyclonal MFF (clone 17090-1-AP, 1:2000; Proteintech), chicken polyclonal Tuj1 (1:1000; Aves), rabbit polyclonal GFP (clone ab6556, cross-reacts with Mito-CFP and amplifies its signal, 1:1000; Abcam). Horseradish peroxidase-conjugated secondary antibodies (1:2000) were from GE Healthcare. For quantification, images were scanned and measured for pixel intensity using NIH ImageJ software, and normalized against β-actin values.

For fluorescence microscopy, cells were cultured on poly-D-lysine-coated Thermanox plastic coverslips (Nalge Nunc International), fixed, permeabilized, and processed for MitoDsRed2 fluorescence imaging or for immunostaining as described previously (Xiang et al., 1996). Fluorescent microscopic images were captured on an Axiovert 200 inverted microscope (Carl Zeiss Microimaging) equipped with a cooled CCD camera (SensiCam). Primary antibodies used were mouse monoclonal Bif-1 (clone 30A882.1.1, 1:500; Imgenex) and chicken Tuj1 (1:500; Aves). The neuronal identity of cells was confirmed by immunostaining for the neuronal marker Tuj1. Nuclei were labeled with Hoechst 33258 (2.5 μg/ml). AlexaFluor dye-conjugated secondary antibodies (1:400) were from Invitrogen. Fluorescent images of MitoDsRed2 were deconvolved using Slidebook (Intelligent Imaging Innovations) and exported out with the γ factor set at 0.7 for better visualization of mitochondrial morphology. Neuritic mitochondrial length was measured using ImageJ, with three random fields counted per experiment (3 experiments total) by an observer blinded to the treatment conditions and averaged.

The JC-1 dye (final concentration 1 μM; Invitrogen), diluted into Ca^{2+}, Mg^{2+}-containing Hanks balanced salt solution (HBSS(+); Invitrogen) from 1 mM stock in DMSO, was applied to live neurons for 20 min at 37°C in a CO_2 incubator. After washing with HBSS (+), fluorescence images were captured on an Axiovert 200 inverted microscope. The mitochondrial uncoupler carbonyl cyanide p-(tri-fluromethoxy)phenylhydrazone (FCCP) was used as a positive control (data not shown) for dissipating mitochondrial membrane potential. With this method, mitochondrial depolarization is reported as a decrease in the red (590 nm) to green (530 nm) fluorescence intensity ratio. Five images per condition were taken at 32× magnification, and the total pixel intensity of red and green fluorescence was obtained to calculate the ratio of red versus green.

MCAO model of stroke. Male Bif-1 $^{+/+}$ and Bif-1 $^{-/-}$ mice (25–30 g; ~12 weeks old) were subjected to middle cerebral artery occlusion (MCAO) as previously described, with a 45 min occlusion time (Baltan et al., 2011). Successful occlusion and reperfusion was confirmed using a Laser Doppler Perfusion Monitor (Moor Instruments). Following 2 d of recovery, brains were removed and nine 1 mm slices were made for 2,3,5-triphenyltetrazolium chloride (TTC) staining to measure infarct volume (Gibson et al., 2005). From a separate cohort of animals, which express Mito-CFP, cortical tissue dorsal to the infarct was dissected out by reference to TTC-stained adjacent slices, and protein lysates were prepared by sonication in SDS buffer (2% SDS, 10% glycerol, 50 mM Tris-Cl, pH 6.8). For tissue immunofluorescence, 35 μm frozen sections were cut on a Leica cryostat and processed similarly to cell culture immunofluorescence, as previously described (Xiang et al., 1996). Primary antibody used was rabbit anti-glial fibrillary acidic protein (GFAP; 1:200, no. G2969, Sigma-Aldrich).

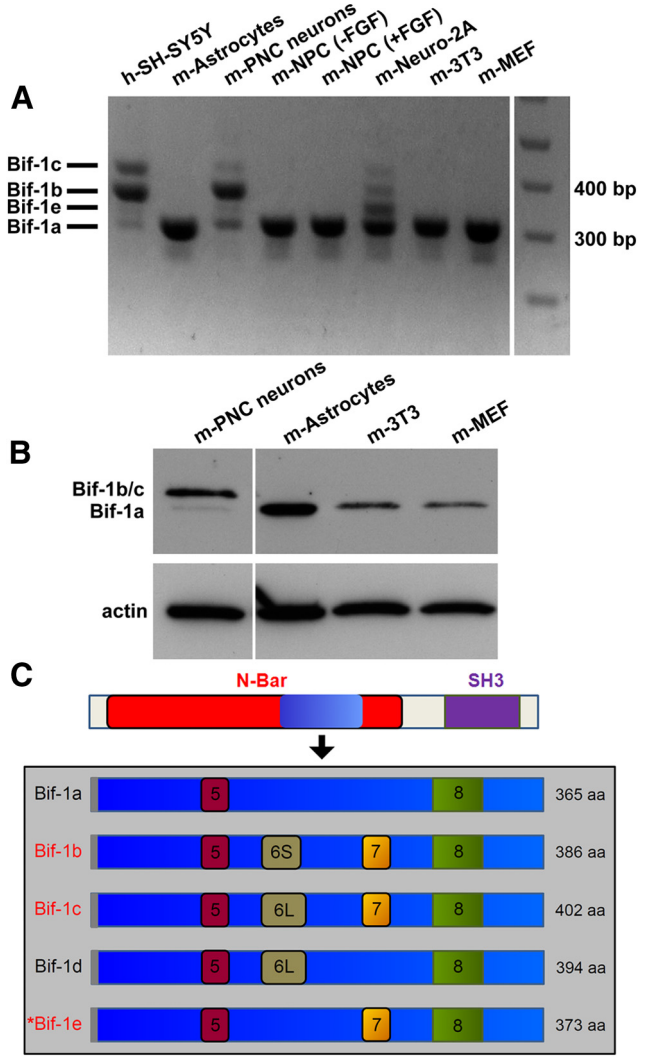

Figure 4. Bif-1 expression in neuronal and non-neuronal cells. ***A***, Primary neurons and neuronal cell lines contain two specific alternatively spliced mRNA isoforms, *Bif-1*b and *Bif-1*c, not expressed in other cell types. Expression levels of *Bif-1* mRNA were analyzed by RT-PCR using primers flanking exons 6 and 7, the sites of alternative *Bif-1* splicing. The same amount of RNA per sample was used for RT-PCR and the same amount of reaction product was loaded to the gel. ***B***, Neurons predominantly express the neuron-specific isoforms of Bif-1 protein. Expression of Bif-1 protein was analyzed by Western blot using a non-isoform-specific antibody. Neuron-specific isoforms (Bif-1b/c) are not separable under the conditions used. h-SH-SY5Y, Human neuroblastoma cell line; m-PNC neurons, mouse postnatal cortical neurons; m-NPC, mouse neural progenitor cells derived from spinal cord; FGF, fibroblast growth factor; m-Neuro-2A, mouse neuroblastoma cell line; m-NIH3T3, mouse fibroblast cell line; m-MEF, mouse embryonic fibroblasts. All samples were run on the same immunoblot and were continuous. The vertical white line indicates an irrelevant lane that was removed from the blot. ***C***, Schematic showing the exon structures of the various Bif-1 isoforms. All splice sites are located within the N-BAR domain, which is responsible for Bif-1 membrane binding function. Neuron-specific isoforms are highlighted in red. *See text under subheading "Neurons specifically express longer, alternatively spliced isoforms of Bif-1" for an explanation of Bif-1e.

Electron microscopy. Cortical neurons were plated on Aclar plastic coverslips coated with poly-D-lysine. Three days after lentiviral infection, cultures were fixed with 2.5% glutaraldehyde in 0.1 M cacodylate buffer. Fixed cultures were prepared for electron microscopy as previously described (Wang et al., 2013). For mitochondrial size measurements, electron micrographs from regions containing only neurites were obtained using a Philips CM10 transmission electron

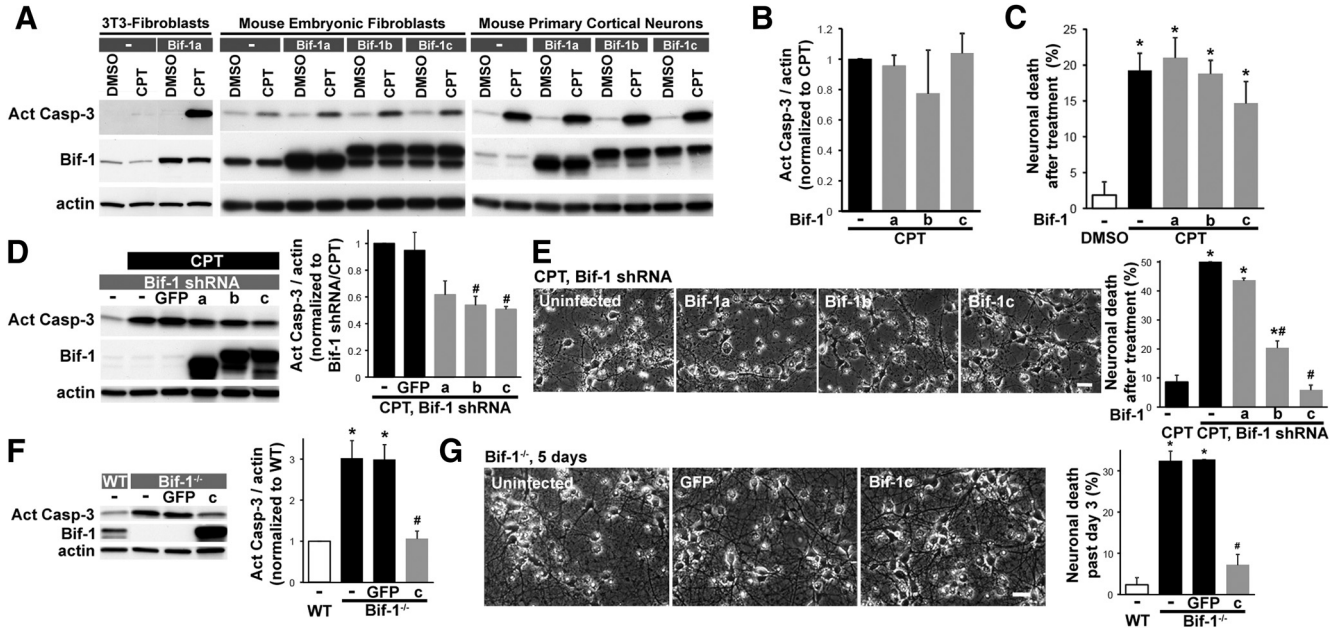

Figure 5. Neuron-specific Bif-1 isoforms (Bif-1b and Bif-1c) can restore neuronal viability in Bif-1-depleted neurons. ***A***, Overexpression of Bif-1 is proapoptotic in fibroblasts, but has no effect on CPT-induced caspase activation in neurons. Fibroblasts (3T3 or mouse embryonic) overexpressing Bif-1 displayed increased levels of activated caspase-3, a measure of apoptosis, following CPT treatment (100 μM as fibroblasts are more resistant to CPT; 12 h), whereas neurons overexpressing various Bif-1 isoforms showed similar basal (DMSO) and CPT (5 μM, 12 h)-induced levels of activated caspase-3 compared with uninfected neurons. ***B***, ***C***, Bif-1 overexpression in neurons has no significant effect on CPT-induced caspase-3 activation (***B***) or cell death (***C***). Activated caspase-3 densitometric results were first normalized against actin and then presented relative to CPT-treated cultures. Bars represent mean ± SEM; *$p < 0.05$ versus DMSO control. ***D***, Overexpression of neuron-specific Bif-1b and Bif-1c reduce caspase-3 activation induced by CPT in the absence of endogenous Bif-1. Neurons were infected with Bif-1 shRNA along with GFP or the Bif-1 isoforms indicated for 3 d before addition of CPT. Bars represent mean ± SEM. Activated caspase-3 levels are shown relative to Bif-1 shRNA/CPT treated cultures; #$p < 0.05$ versus Bif-1 shRNA/GFP/CPT. ***E***, Overexpression of neuron-specific Bif-1b and Bif-1c reduce neuronal death induced by CPT in the absence of Bif-1. Bars represent mean ± SEM; *$p < 0.05$ versus CPT; #$p < 0.05$ versus CPT/Bif-1 shRNA. ***F***, Overexpression of neuron-specific Bif-1c help 5-d-old Bif-1 $^{-/-}$ neuronal cultures maintain basal levels of caspase-3 activation. Activated caspase-3 levels are shown relative to WT cultures at day 5. Bars represent mean ± SEM; *$p < 0.05$ versus WT cultures; #$p < 0.05$ versus GFP-treated Bif-1 $^{-/-}$ cultures. ***G***, Overexpression of neuron-specific Bif-1c reduces neuronal death in 5-d-old Bif-1 $^{-/-}$ neuronal cultures. Bars represent mean ± SEM; *$p < 0.05$ versus WT cultures; #$p < 0.05$ versus GFP-treated Bif-1 $^{-/-}$ cultures. Scale bars: ***E***, ***G***, 25 μm. All images and blots are representative of 2–3 separate experiments that were used for quantification to obtain mean ± SEM. values. Statistics were done with one-way ANOVA with Tukey *post hoc* test. The symbol "—" indicates no addition/treatment.

microscope at 20,000× magnification. Mitochondrial length was measured by placing a tip-to-tip line across the longest axis of each mitochondrion using the straight-line tool in NIH ImageJ. Images with <5 neuritic mitochondria were discarded. For the number of mitochondria per unit area, images were taken of random fields containing neurites at 10,000× magnification. The total number of neuritic mitochondria was divided by the neurite area for each random field. Both measurements (mean mitochondrial length and number of mitochondria per unit area) represent 150–200 mitochondria counted for each experimental condition.

Statistics. Student's *t* tests, one-way and two-way ANOVA with Tukey *post hoc* tests were used where applicable. Results were considered statistically significant when $p \leq 0.05$ using Prism software (GraphPad).

Results

Bif-1 enhances neuronal viability

Neuronal apoptosis mediated by p53 is Bax-dependent (Xiang et al., 1998) and involves changes in mitochondrial dynamics (elongation) that are not seen in non-neuronal cells (Uo et al., 2007; Wang et al., 2013). Bax promotes mitochondrial apoptosis and also regulates mitochondrial dynamics (Xiang et al., 1998; Karbowski et al., 2002, 2004a; Steckley et al., 2007), and Bif-1 has been shown to bind and activate Bax upon apoptosis induction in non-neuronal cells while also promoting mitochondrial fragmentation (Karbowski et al., 2004b; Takahashi et al., 2005). Here, we sought to determine whether Bif-1 also plays a role in mediating a p53-Bax apoptotic pathway in neurons.

CPT is a topoisomerase I inhibitor that causes DNA damage and activates p53 to induce apoptosis in a number of cell types, including neurons (Xiang et al., 1996, 1998; Uo et al., 2007; Wang et al., 2013). Treatment with CPT for 12 h increased morphologically discernible cell death only minimally over DMSO control (Fig. 1*A*), but did promote a significant increase in caspase-3 activation, indicating that neurons were undergoing apoptosis (Fig. 1*B*). Under these conditions, however, Bif-1 protein levels remained unchanged in CPT-treated neurons (Fig. 1*B*, blot; lanes 1 and 2, 96.6 ± 7.1% relative to control treated, $n = 10$), contrary to previous studies with non-neuronal cells showing that Bif-1 levels increase during apoptotic conditions (Yang et al., 2010). shRNA-mediated knockdown was used to assess what role Bif-1 plays in these neurons undergoing apoptosis. Bif-1 knockdown alone did not immediately cause significant changes in neuronal viability (3.5 d after infection; Fig. 1*A*) and elevated activated caspase-3 levels only slightly (Fig. 1*B*). A constitutive prosurvival role for Bif-1 became evident when knockdown neurons (3 d after infection) were challenged with CPT. In these knockdown neurons, CPT treatment resulted in not only a further increase in caspase-3 activation (Fig. 1*B*) but also a significant induction of cell death at 12 h of treatment, when there was only a small increase in cell death in control shRNA virus-infected neurons (Fig. 1*A*). Neuronal cultures from Bif-1 $^{-/-}$ mice were also more sensitive to CPT compared with neurons from Bif-1 $^{+/+}$ mice, which did not show any significant neu-

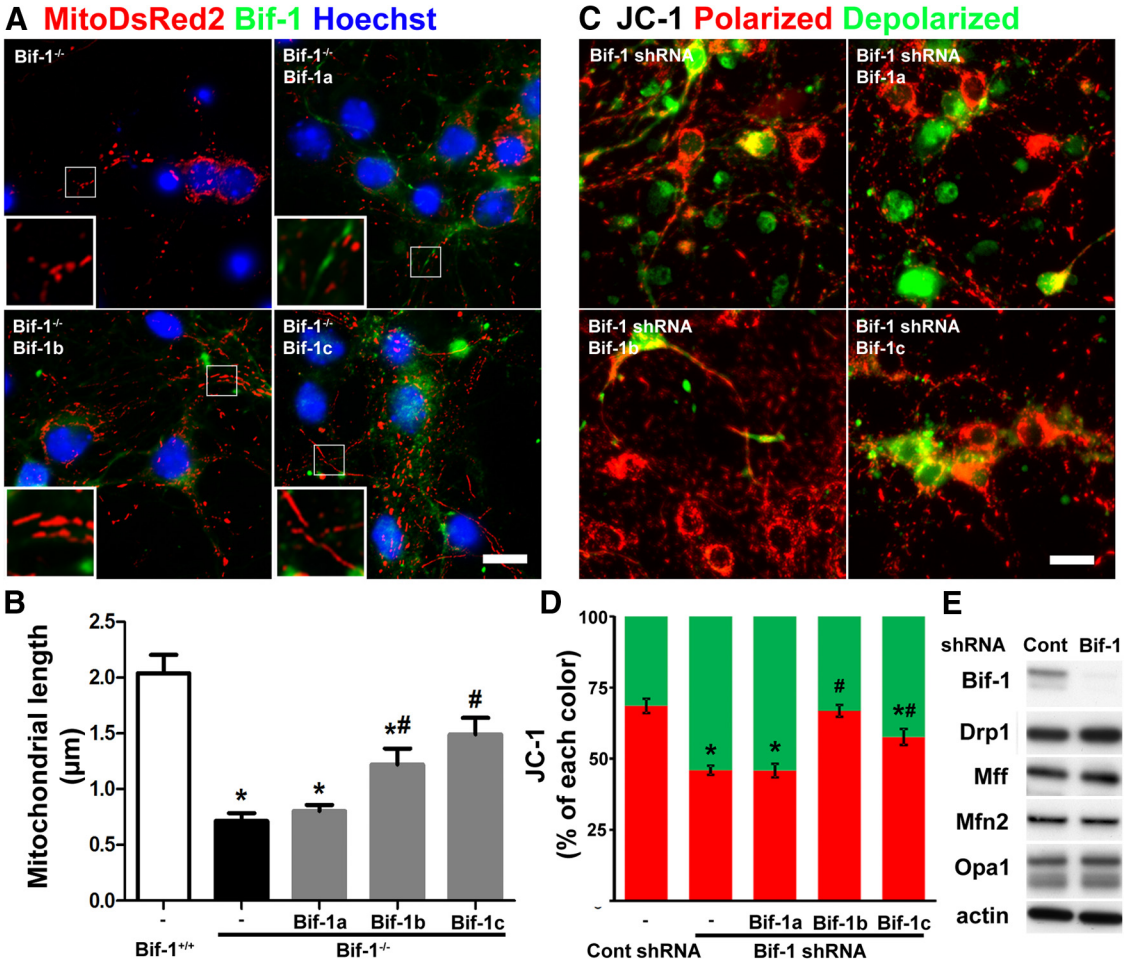

Figure 6. Overexpression of neuron-specific Bif-1 isoforms (Bif-1b and Bif-1c), but not the ubiquitous Bif-1a, can restore mitochondrial shape and function in Bif-1-depleted neurons. ***A***, ***B***, Overexpression of neuron-specific Bif-1b and Bif-1c attenuates the decrease in mitochondrial size caused by the absence of endogenous Bif-1. Neurons from Bif-1 deficient mice were infected with the Bif-1 isoforms indicated along with MitoDsRed2 to visualize changes in mitochondrial morphology at 3 d after infection. Bif-1c localization was more punctate, in contrast with the more uniformly cytosolic distribution of Bif-1a and Bif-1b. Average mitochondrial length per image was measured using ImageJ by an observer blinded to the treatment conditions. Bars represent mean ± SEM; $*p < 0.05$ versus Bif-1 $^{+/+}$ cultures; $\#p < 0.05$ versus Bif-1 $^{-/-}$ cultures. ***C***, ***D***, Overexpression of neuron-specific Bif-1b and Bif-1c attenuate mitochondrial depolarization caused by endogenous Bif-1 knockdown. The data are presented as the relative ratio (percentage) of red and green fluorescence intensity to indicate changes in the overall mitochondrial membrane potential. Bars represent mean ± SEM; $*p < 0.05$ versus control shRNA; $\#p < 0.05$ versus Bif-1 shRNA. ***E***, Bif-1 knockdown does not affect other proteins involved in the maintenance of mitochondrial morphology. Immunoblot analysis of protein extracts obtained at 3 d after Bif-1 shRNA infection. Scale bars: ***A***, 10 μm; ***C***, 20 μm. All images and blots are representative of three separate experiments. White bordered insets demarcate areas that were magnified threefold. Statistics were done with one-way ANOVA with Tukey *post hoc* test.

ronal death (Fig. 1*C*). Significant neuron loss was eventually observed by day 5 in both Bif-1 $^{-/-}$ neurons and wild-type neurons treated with Bif-1 shRNA, relative to controls, which did not contain any significant cell death between days 3 and 5 (Fig. 1*D*).

Bif-1 promotes mitochondrial elongation in neurons

Because Bif-1 exerted a contrasting effect on apoptosis in neurons compared with its reported effects in non-neuronal cell types, we next investigated the influence of Bif-1 on mitochondrial morphology in neurons. This was accomplished by visualizing MitoDsRed2 fluorescence in the neuritic compartment where individual mitochondria are more readily discernible. Bif-1 $^{-/-}$ neurons displayed greatly reduced numbers of mitochondria in neurites and their lengths were also substantially shorter compared with neurons from Bif-1 $^{+/+}$ mice (Fig. 2*A*). Although mitochondria in the cell bodies in Bif-1 $^{-/-}$ neurons were difficult to distinguish individually due to mitochondrial aggregation, they also appeared smaller and more punctate, when compared with Bif-1 $^{+/+}$ neurons (Fig. 2*A*).

Bif-1 knockdown in wild-type neurons was then used to validate the observations seen in Bif-1 $^{-/-}$ neurons. Bif-1 shRNA-infected neurons displayed highly fragmented mitochondria that were almost exclusively perinuclear (Fig. 2*B*), similar to the phenotype observed with Mfn2 knockdown which is known to promote mitochondrial fission in neurons (Uo et al., 2009; Pham et al., 2012). Bif-1 knockdown also induced mitochondrial depolarization, as visualized by a shift in JC-1 fluorescence from red to green (Fig. 2*C*), similar to the effect generated by treatment with the mitochondrial uncoupler FCCP (Fig. 2*C*, inset), suggesting that loss of Bif-1 in neurons compromises mitochondrial bioenergetic function.

Electron microscopy (EM) analysis of mitochondrial size in neurites revealed smaller mitochondria in both Bif-1 deficient (Fig. 3*A*,*B*) and Bif-1-depleted neurons (Fig. 3*A*,*D*), and confirmed that there were fewer mitochondria present in Bif-1-deficient neurons (Fig. 3*B*). Accumulation of smaller mitochondria at the expense of larger mitochondria is evident from analysis of mitochondrial size distribution in Bif-1-deficient neurons (Fig. 3*C*).

In contrast to its effect on mitochondrial morphology in neurons, Bif-1 knockdown in mouse embryonic fibroblasts resulted in more elongated, interconnected mitochondria (Fig. 2*D*), consistent with previous results in non-neuronal cells (Karbowski et al., 2004b; Takahashi et al., 2013), whereas Mfn2 knockdown again resulted in smaller, fragmented mitochondria. Thus, although Mfn2 behaves as a fusion protein in both neurons and fibroblasts, Bif-1 exerts disparate effects on mitochondrial morphology between neurons and non-neuronal cells.

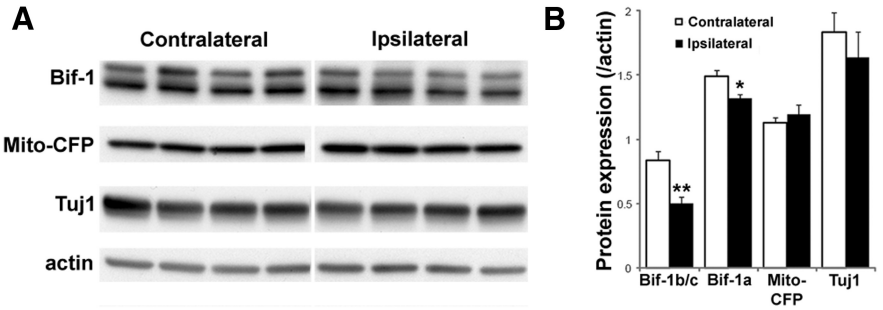

Figure 7. Bif-1 expression is decreased in the penumbra after focal transient ischemia. ***A***, Mito-CFP mice (Bif-1 wild-type) were subjected to MCAO for 45 min. After 2 d, tissue dorsal to the infarct (visualized by TTC in adjacent slices) was analyzed for protein expression. The corresponding region of tissue from the contralateral side was taken as a control. Data from four different animals are shown with some irrelevant lanes cutoff in the middle of the blot. ***B***, Densitometric quantification of the Western blots. Bars represent mean ± SEM; $*p < 0.05$, $**p < 0.01$, Student's *t* test ($n = 4$ animals per condition).

Neurons specifically express longer, alternatively spliced isoforms of Bif-1

The contrasting effects of Bif-1 knockdown observed in neurons versus non-neuronal cells may result from the selective expression of unique Bif-1 isoforms in neurons. It has been previously reported that different Bif-1 isoforms exist in brain (Modregger et al., 2003). Using RT-PCR (Fig. 4*A*) and Western blot analysis (Fig. 4*B*), we demonstrated that only neurons and neuroblastoma cells expressed longer isoforms of Bif-1 message and protein. In contrast, all other cell types tested, including fibroblasts, astrocytes and neural progenitor cells, expressed only the shortest isoform, Bif-1a (Fig. 4). Although the mRNA sequences for the various isoforms were resolvable (Fig. 4*A*), our protein blots (Fig. 4*B*) were only able to differentiate between neuron-specific isoforms showing up as a single band (Bif-1b/c) and the ubiquitous isoform (Bif-1a). However, the relative mRNA levels of the Bif-1 isoforms suggest that in mouse primary neurons Bif-1b is preferentially expressed over the other neuron-specific forms (Fig. 4*A*). Thus, although the larger protein band found in neurons (Bif-1b/c; Fig. 4*B*) is likely to be predominantly Bif-1b, we use Bif-1b/c throughout this study.

DNA sequence analysis of these differentially spliced isoforms confirmed that the splicing events in neurons involve inclusion/exclusion of exons 6 and 7, located within the N-BAR domain, which is responsible for the membrane binding and curvature function of Bif-1 (Modregger et al., 2003). A diagram depicting the different Bif-1 isoforms is shown in Figure 4*C*. The ubiquitously expressed Bif-1a is the shortest, lacking exons 6 and 7, whereas Bif-1c is the longest, containing both exons. Bif-1b differs from Bif-1c in that it contains a short (39 bp) form of exon 6 (6S) rather than the long (89 bp) form (6 L). Curiously, although Bif-1a and Bif-1b were found in multiple sequence databases, Bif-1c was absent; instead, a different isoform (NM_001206651.1 transcript variant 2, which we designate Bif-1d) was found, which contains full-length exon 6 but lacks exon 7. We were unable to detect the expression of Bif-1d mRNA, however, in either mouse neurons or whole mouse and human cortical brain homogenates using PCR primers that would specifically amplify this isoform. Neurons and neuroblastoma cells expressed an additional isoform that contains exon 7 but lacks exon 6; a search of the NCBI database revealed one mRNA transcript that contains this sequence (XM_004752659.1, which we designate Bif-1e). The presence of neuron-specific isoforms that involve alternative usage of exons 6 and 7 in the N-BAR domain suggest that neuron-specific functions of Bif-1 may potentially involve its modified ability to bind and manipulate membranes.

Neuron-specific isoforms (Bif-1b and Bif-1c) attenuate neuronal death and mitochondrial deficits induced by Bif-1 knockdown

We next examined whether discrete Bif-1 isoforms displayed different activities or functions in neurons. Overexpression of different human Bif-1 isoforms had no effect on CPT-induced cell death in mouse primary cortical neurons (Fig. 5*A–C*). In contrast, Bif-1 overexpression in both mouse embryonic fibroblasts and NIH3T3-fibroblasts augmented CPT-induced apoptosis as judged by caspase-3 activation (Fig. 5*A*), consistent with previous reports of Bif-1 being a proapoptotic protein in non-neuronal cells (Takahashi et al., 2005). However, the differential functions of neuron-specific Bif-1 isoforms became evident when endogenous Bif-1 was eliminated by shRNA treatment. Overexpression of neuron-specific Bif-1b or Bif-1c in Bif-1 shRNA-treated neurons attenuated CPT-induced caspase-3 activation (Fig. 5*D*) and cell death (Fig. 5*E*) augmented by Bif-1 knockdown, whereas the ubiquitous isoform, Bif-1a, lacked this ability (Fig. 5*D*,*E*). These human Bif-1 isoform constructs were resistant to the mouse Bif-1 shRNA sequence, as validated by Western blot (Fig. 5*D*). Overexpression of Bif-1c also attenuated naturally occurring apoptosis and neuronal death in 5-d-old Bif-1 $^{-/-}$ neuron cultures (Fig. 5*F*,*G*).

In Bif-1 $^{-/-}$ neurons that contain smaller mitochondria than WT neurons, overexpression of neuron-specific Bif-1b and c isoforms, but not ubiquitous Bif-1a, increased mitochondrial length as visualized by MitoDsRed2 fluorescence microscopy (Fig. 6*A*,*B*). The intracellular distribution of overexpressed isoform c protein appeared more punctate than the other two isoforms, which only exhibited a diffuse distribution in both the cell body and neurites (Fig. 6*A*). However, it was rare to observe specific colocalization of any Bif-1 isoform with mitochondrial markers (MitoDsRed2 or Tom20, data not shown) in neurons. Similarly, only Bif-1b and Bif-1c were able to attenuate Bif-1 shRNA-induced mitochondrial depolarization, visualized by JC-1 staining (Fig. 6*C*,*D*). These mitochondrial abnormalities caused by Bif-1 knockdown were not due to alterations in expression levels of proteins commonly associated with maintenance of mitochondrial morphology, including the fission proteins Drp1 and mitochondrial fission factor (Mff) and the fusion proteins Mfn2 and optic atrophy 1 (Opa1; Fig. 6*E*).

Bif-1 $^{-/-}$ mice are more vulnerable to ischemic injury

Based upon our *in vitro* findings, we sought to determine, using an *in vivo* model of neuronal stress, if Bif-1 was in fact required to maintain neuronal viability. Because Bif-1 expression increases

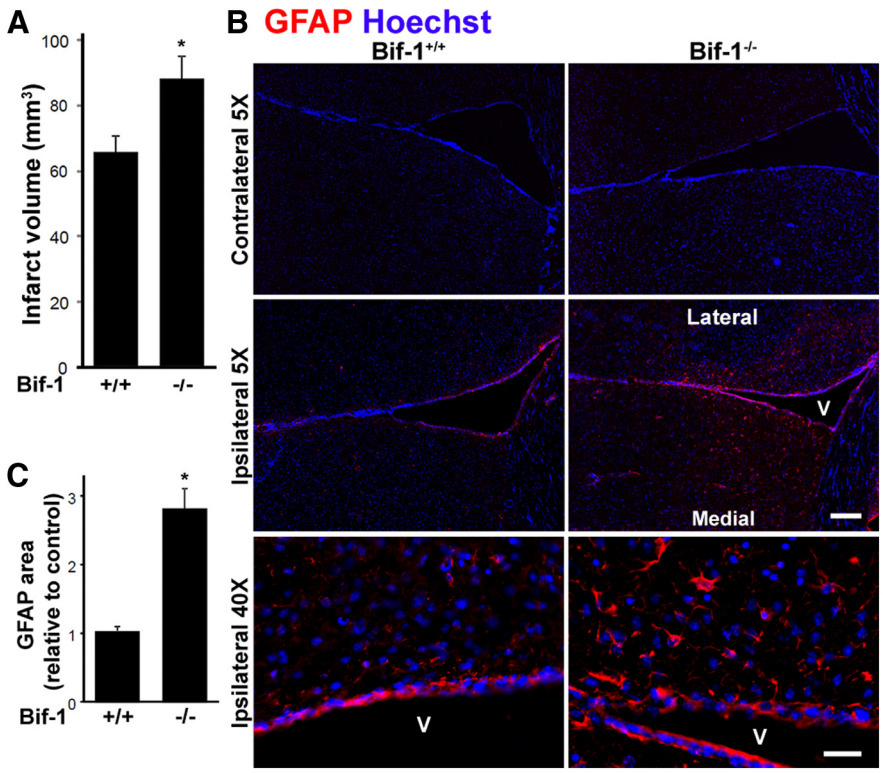

Figure 8. Bif-1 $^{-/-}$ mice show increased sensitivity to ischemic injury in the MCAO model. ***A***, Bif-1 $^{-/-}$ animals had larger infarct volumes after MCAO injury (45 min occlusion, 2 d reperfusion) than Bif-1 $^{+/+}$ controls. Infarct volume was determined by TTC staining of serial coronal slices as described in Materials and Methods. Bars represent mean ± SEM; $*p < 0.05$, Student's *t* test ($N = 10$ animals per condition). ***B***, Bif1 $^{-/-}$ animals show exaggerated astrogliosis after MCAO injury. Micrographs of coronal sections through the striatum are shown for GFAP immunoreactivity (red) visualizing astrocytes. Two days after MCAO injury, astrocytes around the infarct are seen further medially toward the medial septum in Bif1 $^{-/-}$ animals, corresponding to a larger infarct volume. Astrocytes around the infarct in Bif1 $^{-/-}$ animals were larger with longer ramified processes, a morphology typical of reactive astrocytes compared with wild-type animals. Nuclei are visualized with Hoechst 33258 dye (blue). Scale bar: ***B*** (5×), 200 μm; ***B*** (40×), 20 μm. V, Ventricle. ***C***, GFAP immunoreactivity on the ipsilateral side was quantified using Slidebook and normalized relative to Bif-1 $^{+/+}$ mice. Bars represent mean ± SEM; $*p < 0.05$, Student's *t* test ($n = 4$ animals per condition).

under conditions of cell death in non-neuronal cells where Bif-1 is proapoptotic (Yang et al., 2010), we reasoned that Bif-1 expression may decrease in stressed neurons where Bif-1 is expected to be prosurvival. We used the MCAO model of ischemic injury to test this, using Bif-1 wild-type mice expressing Mito-CFP under the neuron-specific Thy1 promoter (Misgeld et al., 2007). Two days postsurgery, cortical tissue dorsal to the infarct, containing the ischemic penumbra, was dissected out and analyzed for Bif-1 protein expression, with the corresponding unaffected contralateral region used as a control. As expected, both Bif-1a and Bif-1b/c expression was decreased, with the neuron-specific isoform showing a greater reduction (Fig. 7). This was not due to neuronal cell loss as there was essentially no decrease in the neuron-specific marker Tuj1 or neuronally expressed Mito-CFP at this time point in the penumbra (Fig. 7).

To validate the hypothesis that the loss of Bif-1 may sensitize neurons to stress-induced death, Bif-1 $^{+/+}$ and Bif-1 $^{-/-}$ mice were subjected to MCAO. At day 2 postsurgery, Bif-1 $^{-/-}$ brains displayed on average a 34.6% larger infarct volume as assessed by TTC staining (Fig. 8*A*), suggesting that neurons lacking Bif-1 were more vulnerable to ischemic injury. Resting astrocytes on the uninjured contralateral side, as visualized by staining for the astrocyte-specific marker GFAP, appeared similar in number and morphology between Bif-1 $^{-/-}$ and Bif-1 $^{+/+}$ animals (Fig. 8*B*). Astrocytes on the injured ipsilateral side, however, appeared more activated in Bif-1 $^{-/-}$ animals based on their overall larger size and number of processes (Fig. 8*B*), consistent with the presence of more extensive underlying neuronal damage. Furthermore, the zone of reactive astrocytes around the infarct was expanded more medially in Bif-1 $^{-/-}$ animals (Fig. 8*B*), resulting in a significant increase in GFAP immunoreactivity around the ventricles (Fig. 8*C*), consistent with their larger infarct volume. Together, these data suggest that Bif-1 is required for maintaining neuronal viability and its loss sensitizes neurons to cell death induced by stress such as ischemic injury.

Discussion

Several studies have shown that Bif-1 is a proapoptotic protein and promotes mitochondrial fragmentation (Cuddeback et al., 2001; Karbowski et al., 2004b; Takahashi et al., 2005; Yang et al., 2010). In the present study, however, we observed that Bif-1 in neurons has the opposite functions. Knockdown of Bif-1 in mouse postnatal cortical neurons enhanced the apoptotic response to DNA damage and elicited mitochondrial fragmentation. Bif-1 knock-out/knockdown neurons in culture contained fragmented mitochondria, particularly in neurites, but restored normal mitochondrial morphology upon Bif-1 overexpression. In a mouse model of stroke, Bif-1 expression was decreased in the penumbra and the stroke outcome was exacerbated in Bif-1 $^{-/-}$ animals, manifesting larger infarct volumes coupled with increased astrocytic activation. These findings support the idea that, in neurons, Bif-1 has prosurvival functions and promotes mitochondrial elongation. Finally, we showed that neurons express unique, longer isoforms of Bif-1, which may partly explain these distinct Bif-1 functions seen between neuronal and non-neuronal cells as evidenced by the observation that only neuron-specific Bif-1 isoforms could attenuate apoptosis sensitivity and mitochondrial deficits induced by Bif-1 suppression.

Bif-1 functions as a prosurvival factor in neurons

The mechanism by which Bif-1 promotes viability in neurons has not been elucidated, but the proapoptotic function in non-neuronal cells is thought to involve its binding to and activation of Bax and Bak (Cuddeback et al., 2001; Takahashi et al., 2005). Induction of apoptosis leads to Bif-1 association with Bax on mitochondria and a conformational change in Bax (Cuddeback et al., 2001; Takahashi et al., 2005) as well as an increase in Bif-1 expression (Yang et al., 2010). Additionally, overexpression of Bif-1 during apoptosis promotes a Bax conformational change and enhances apoptosis (Cuddeback et al., 2001), whereas knockdown of Bif-1 prevents the activation of both Bax and Bak (Takahashi et al., 2005). In non-neuronal cells, p53 can directly bind and activate Bax to trigger apoptosis (Chipuk et al., 2004), whereas in neurons, Bax activation may be restricted through p53 transcriptional activation of PUMA (Uo et al., 2007). In addition,

neurons do not express full-length Bak, but rather an alternatively spliced, BH3 domain-only form of Bak (Uo et al., 2005; Jakobson et al., 2012), which may not be subject to regulation by Bif-1. These key differences in the apoptotic pathways mediated by Bax/Bak in neurons may explain, in part, the opposing actions Bif-1 exerts on cell death and survival between neuronal and non-neuronal cells.

There have been few studies on Bif-1 in neurons. In PC-12 cells, Bif-1 has been shown to be involved in nerve growth factor receptor trafficking, a key regulatory event in neuronal survival and differentiation (Wan et al., 2008). Bif-1 knockdown resulted in NGF receptor degradation, attenuation of Erk signaling, and inhibition of neurite outgrowth (Wan et al., 2008). It is possible that knockdown of Bif-1 could prevent neurons from receiving prosurvival signals, resulting in enhanced sensitivity to injury. However, the same group demonstrated that Bif-1 knockdown attenuated 1-methyl-4-phenylpyridinium (MPP^+) and mutant α-synuclein-mediated cell death in cultured cortical neurons (Wong et al., 2011). One explanation is that, depending on the type of neurotoxic insult, Bif-1 levels or activity can either decrease (as with stroke; Fig. 7) or increase (Wong et al., 2011); normalization of Bif-1 function in either direction could then be neuroprotective. This may explain why overexpression of Bif-1 did not protect against CPT-induced apoptosis in neurons (Fig. 5*A–C*), because CPT did not induce a decrease in Bif-1 (Fig. 1), whereas neuron-specific Bif-1 isoforms did counteract increases in sensitivity to CPT-induced apoptosis caused by Bif-1 knockdown (Fig. 5*D*,*E*). Another possibility relates to the mechanisms of cell death; in Parkinson's disease, abnormally increased autophagy is thought to be a causative factor in neuronal death (Wong et al., 2011), while in stroke, studies have shown autophagy to be neuroprotective (Papadakis et al., 2013). Examining Bif-1 expression in other neurodegenerative diseases, such as Alzheimer's disease, may lead to new insights regarding how Bif-1 functions to promote neuronal survival or apoptosis.

In the MCAO model of stroke, Bif-1 levels decreased in the ischemic penumbra (Fig. 7), an area where neurons may either recover or undergo apoptosis (del Zoppo et al., 2011). The decrease was greater for neuron-specific isoforms (Bif-1b/c) than for Bif-1a, suggesting that this was mainly a neuronal event. This decrease at day 2 post-MCAO occurred with no neuronal death yet taking place, as indicated by the lack of change in the levels of the neuron-specific marker Tuj1 or neuron-specific Mito-CFP. Along with the larger infarcts observed in Bif-$1^{-/-}$ animals, this drop in Bif-1 expression preceding the potential neuronal death that could ensue in the penumbra points to the possibility that Bif-1 plays a prosurvival role for neurons, and decreased Bif-1 expression is causal to increased vulnerability of neurons to apoptotic stress. We also observed enhanced astrocytic activation in response to MCAO in Bif-$1^{-/-}$ animals. Although this likely represents a glial response to greater neuronal damage precipitating in the absence of Bif-1, we cannot rule out the possibility that Bif-1 also plays a role in intrinsic glial responses to ischemic conditions that can either counteract or exacerbate neuronal stress. Neuron or glia-specific overexpression or knock-out of Bif-1 could address this issue.

Loss of Bif-1 in neurons resulted in fragmented mitochondria

Bif-1 knockdown/knock-out neurons displayed smaller mitochondria, most noticeably in neurites where individual mitochondria can be readily discerned (Fig. 2). EM analysis of cultured neurons corroborated these results and further showed the presence of very small (fragmented) mitochondria (Fig. 3). Conversely, overexpression of Bif-1 restored a normal mitochondrial phenotype in Bif-$1^{-/-}$ neurons, but in an isoform-specific manner with the neuron-specific isoforms, Bif-1b and Bif-1c, being more efficacious than the ubiquitously expressed Bif-1a (Fig. 6). Consistent with the failed maintenance of mitochondrial morphology, mitochondrial membrane potential in Bif-1 knockdown neurons was found to be compromised (Fig. 2*C*). Thus, in sharp contrast to its function in non-neuronal cells, Bif-1 or, more specifically, neuron-specific Bif-1 isoforms in neurons appear to be required for maintaining the size and bioenergetic function of mitochondria. It comes as no surprise, therefore, that when put under stress (DNA damage, MCAO), Bif-1 knock-out/knockdown neurons exhibit an exacerbated apoptotic outcome. Even in the absence of experimental stress, neurons succumbed to spontaneous cell death when reduced levels of Bif-1 (by knockout or knockdown) are maintained for 5 d in culture (Figs. 1*D*, 5*F*,*G*), pointing to the essential contribution of Bif-1 to neuronal viability. These results suggest that the ability of Bif-1 to modulate mitochondrial morphology and bioenergetic capabilities may have direct implications for its prosurvival action in neurons.

Interestingly, Bif-1 deficiency also resulted in fewer total mitochondria in neurites, as confirmed by EM (Fig. 3). If Bif-1 deficiency does indeed result in increased mitochondrial fission, one would expect a larger number of small mitochondria, keeping the overall mitochondrial volume constant, but this was not the case. It is possible that smaller mitochondria resulting from Bif-1 deficiency are selectively targeted for degradation. Although it is unknown exactly how mitochondria in Bif-1-deficient neurons become smaller, it appears that Bif-1 does not influence mitochondrial fusion rates directly (Karbowski et al., 2004b). Because we did not observe changes in the expression of fusion (Mfn2, Opa1) or fission proteins (Drp1, Mff) in response to Bif-1 knockdown (Fig. 6*E*), it is conceivable that Bif-1 influences the activity of fission proteins.

Concluding remarks

Depletion of Bif-1 in neurons resulted in smaller, fragmented mitochondria and increased sensitivity to neurotoxic stress. Although it did not lead to an immediate decline in viability, loss of Bif-1 expression compromised mitochondrial function and raised neuronal sensitivity to neurotoxic insults *in vitro* (camptothecin) and *in vivo* (MCAO). The data obtained in the current study show that Bif-1 acts as a prosurvival factor in neurons at least in part by maintaining mitochondrial integrity in sharp contrast to the proapoptotic function previously reported for this protein in non-neuronal cells. Early detection of lowered Bif-1 expression and subsequent restoration may prove useful in mitigating neuronal dysfunction and death in nervous system injury and disease.

References

Baltan S, Bachleda A, Morrison RS, Murphy SP (2011) Expression of histone deacetylases in cellular compartments of the mouse brain and the effects of ischemia. Transl Stroke Res 2:411–423. CrossRef Medline

Bertholet AM, Millet AM, Guillermin O, Daloyau M, Davezac N, Miquel MC, Belenguer P (2013) OPA1 loss of function affects in vitro neuronal maturation. Brain 136:1518–1533. CrossRef Medline

Chipuk JE, Kuwana T, Bouchier-Hayes L, Droin NM, Newmeyer DD, Schuler M, Green DR (2004) Direct activation of Bax by p53 mediates mitochondrial membrane permeabilization and apoptosis. Science 303:1010–1014. CrossRef Medline

Cuddeback SM, Yamaguchi H, Komatsu K, Miyashita T, Yamada M, Wu C, Singh S, Wang HG (2001) Molecular cloning and characterization of

Bif-1: a novel Src homology 3 domain-containing protein that associates with Bax. J Biol Chem 276:20559–20565. CrossRef Medline

del Zoppo GJ, Sharp FR, Heiss WD, Albers GW (2011) Heterogeneity in the penumbra. J Cereb Blood Flow Metab 31:1836–1851. CrossRef Medline

Delettre C, Lenaers G, Griffoin JM, Gigarel N, Lorenzo C, Belenguer P, Pelloquin L, Grosgeorge J, Turc-Carel C, Perret E, Astarie-Dequeker C, Lasquellec L, Arnaud B, Ducommun B, Kaplan J, Hamel CP (2000) Nuclear gene OPA1, encoding a mitochondrial dynamin-related protein, is mutated in dominant optic atrophy. Nat Genet 26:207–210. CrossRef Medline

Gibson CL, Bath PM, Murphy SP (2005) G-CSF reduces infarct volume and improves functional outcome after transient focal cerebral ischemia in mice. J Cereb Blood Flow Metab 25:431–439. CrossRef Medline

Jakobson M, Lintulahti A, Arumäe U (2012) mRNA for N-Bak, a neuron-specific BH3-only splice isoform of Bak, escapes nonsense-mediated decay and is translationally repressed in the neurons. Cell Death Dis 3:e269. CrossRef Medline

Kageyama Y, Zhang Z, Roda R, Fukaya M, Wakabayashi J, Wakabayashi N, Kensler TW, Reddy PH, Iijima M, Sesaki H (2012) Mitochondrial division ensures the survival of postmitotic neurons by suppressing oxidative damage. J Cell Biol 197:535–551. CrossRef Medline

Karbowski M, Youle RJ (2003) Dynamics of mitochondrial morphology in healthy cells and during apoptosis. Cell Death Differ 10:870–880. CrossRef Medline

Karbowski M, Lee YJ, Gaume B, Jeong SY, Frank S, Nechushtan A, Santel A, Fuller M, Smith CL, Youle RJ (2002) Spatial and temporal association of Bax with mitochondrial fission sites, Drp1, and Mfn2 during apoptosis. J Cell Biol 159:931–938. CrossRef Medline

Karbowski M, Arnoult D, Chen H, Chan DC, Smith CL, Youle RJ (2004a) Quantitation of mitochondrial dynamics by photolabeling of individual organelles shows that mitochondrial fusion is blocked during the Bax activation phase of apoptosis. J Cell Biol 164:493–499. CrossRef Medline

Karbowski M, Jeong SY, Youle RJ (2004b) Endophilin B1 is required for the maintenance of mitochondrial morphology. J Cell Biol 166:1027–1039. CrossRef Medline

Kim J, Moody JP, Edgerly CK, Bordiuk OL, Cormier K, Smith K, Beal MF, Ferrante RJ (2010) Mitochondrial loss, dysfunction and altered dynamics in Huntington's disease. Hum Mol Genet 19:3919–3935. CrossRef Medline

Misgeld T, Kerschensteiner M, Bareyre FM, Burgess RW, Lichtman JW (2007) Imaging axonal transport of mitochondria in vivo. Nat Methods 4:559–561. CrossRef Medline

Modregger J, Schmidt AA, Ritter B, Huttner WB, Plomann M (2003) Characterization of endophilin B1b, a brain-specific membrane-associated lysophosphatidic acid acyl transferase with properties distinct from endophilin A1. J Biol Chem 278:4160–4167. CrossRef Medline

Papadakis M, Hadley G, Xilouri M, Hoyte LC, Nagel S, McMenamin MM, Tsaknakis G, Watt SM, Drakesmith CW, Chen R, Wood MJ, Zhao Z, Kessler B, Vekrellis K, Buchan AM (2013) Tsc1 (hamartin) confers neuroprotection against ischemia by inducing autophagy. Nat Med 19:351–357. CrossRef Medline

Pham AH, Meng S, Chu QN, Chan DC (2012) Loss of Mfn2 results in progressive, retrograde degeneration of dopaminergic neurons in the nigrostriatal circuit. Hum Mol Genet 21:4817–4826. CrossRef Medline

Schon EA, Przedborski S (2011) Mitochondria: the next (neurode)generation. Neuron 70:1033–1053. CrossRef Medline

Steckley D, Karajgikar M, Dale LB, Fuerth B, Swan P, Drummond-Main C, Poulter MO, Ferguson SS, Strasser A, Cregan SP (2007) Puma is a dominant regulator of oxidative stress induced bax activation and neuronal apoptosis. J Neurosci 27:12989–12999. CrossRef Medline

Takahashi Y, Karbowski M, Yamaguchi H, Kazi A, Wu J, Sebti SM, Youle RJ, Wang HG (2005) Loss of Bif-1 suppresses Bax/Bak conformational change and mitochondrial apoptosis. Mol Cell Biol 25:9369–9382. CrossRef Medline

Takahashi Y, Coppola D, Matsushita N, Cualing HD, Sun M, Sato Y, Liang C, Jung JU, Cheng JQ, Mulé JJ, Pledger WJ, Wang HG (2007) Bif-1 interacts with Beclin 1 through UVRAG and regulates autophagy and tumorigenesis. Nat Cell Biol 9:1142–1151. CrossRef Medline

Takahashi Y, Hori T, Cooper TK, Liao J, Desai N, Serfass JM, Young MM, Park S, Izu Y, Wang HG (2013) Bif-1 haploinsufficiency promotes chromosomal instability and accelerates Myc-driven lymphomagenesis via suppression of mitophagy. Blood 121:1622–1632. CrossRef Medline

Uo T, Kinoshita Y, Morrison RS (2005) Neurons exclusively express N-Bak, a BH3 domain-only Bak isoform that promotes neuronal apoptosis. J Biol Chem 280:9065–9073. CrossRef Medline

Uo T, Kinoshita Y, Morrison RS (2007) Apoptotic actions of p53 require transcriptional activation of PUMA and do not involve a direct mitochondrial/cytoplasmic site of action in postnatal cortical neurons. J Neurosci 27:12198–12210. CrossRef Medline

Uo T, Dworzak J, Kinoshita C, Inman DM, Kinoshita Y, Horner PJ, Morrison RS (2009) Drp1 levels constitutively regulate mitochondrial dynamics and cell survival in cortical neurons. Exp Neurol 218:274–285. CrossRef Medline

Wan J, Cheung AY, Fu WY, Wu C, Zhang M, Mobley WC, Cheung ZH, Ip NY (2008) Endophilin B1 as a novel regulator of nerve growth factor/ TrkA trafficking and neurite outgrowth. J Neurosci 28:9002–9012. CrossRef Medline

Wang DB, Garden GA, Kinoshita C, Wyles C, Babazadeh N, Sopher B, Kinoshita Y, Morrison RS (2013) Declines in Drp1 and parkin expression underlie DNA damage-induced changes in mitochondrial length and neuronal death. J Neurosci 33:1357–1365. CrossRef Medline

Wang X, Su B, Lee HG, Li X, Perry G, Smith MA, Zhu X (2009) Impaired balance of mitochondrial fission and fusion in Alzheimer's disease. J Neurosci 29:9090–9103. CrossRef Medline

Waterham HR, Koster J, van Roermund CW, Mooyer PA, Wanders RJ, Leonard JV (2007) A lethal defect of mitochondrial and peroxisomal fission. N Engl J Med 356:1736–1741. CrossRef Medline

Wong AS, Lee RH, Cheung AY, Yeung PK, Chung SK, Cheung ZH, Ip NY (2011) Cdk5-mediated phosphorylation of endophilin B1 is required for induced autophagy in models of Parkinson's disease. Nat Cell Biol 13:568–579. CrossRef Medline

Xiang H, Hochman DW, Saya H, Fujiwara T, Schwartzkroin PA, Morrison RS (1996) Evidence for p53-mediated modulation of neuronal viability. J Neurosci 16:6753–6765. Medline

Xiang H, Kinoshita Y, Knudson CM, Korsmeyer SJ, Schwartzkroin PA, Morrison RS (1998) Bax involvement in p53-mediated neuronal cell death. J Neurosci 18:1363–1373. Medline

Yang J, Takahashi Y, Cheng E, Liu J, Terranova PF, Zhao B, Thrasher JB, Wang HG, Li B (2010) GSK-3β promotes cell survival by modulating Bif-1-dependent autophagy and cell death. J Cell Sci 123:861–870. CrossRef Medline

Züchner S, Mersiyanova IV, Muglia M, Bissar-Tadmouri N, Rochelle J, Dadali EL, Zappia M, Nelis E, Patitucci A, Senderek J, Parman Y, Evgrafov O, Jonghe PD, Takahashi Y, Tsuji S, Pericak-Vance MA, Quattrone A, Battaloglu E, Polyakov AV, Timmerman V, Schröder JM, et al. (2004) Mutations in the mitochondrial GTPase mitofusin 2 cause Charcot-Marie-Tooth neuropathy type 2A. Nat Genet 36:449–451. CrossRef Medline